

Cu-supported nano-ZrZnO_x as a highly active inverse catalyst for low temperature methanol synthesis from CO₂ hydrogenation

Yangzhi Xu ^{a,1}, Zirui Gao ^{b,1}, Yao Xu ^b, Xuetao Qin ^b, Xin Tang ^a, Zhiwei Xie ^a, Jinrong Zhang ^a, Chuqiao Song ^a, Siyu Yao ^c, Wu Zhou ^{d,e,*}, Ding Ma ^{b,***}, Lili Lin ^{a,f,***}

^a Institute of Industrial Catalysis, State Key Laboratory of Green Chemistry Synthesis Technology, College of Chemical Engineering, Zhejiang University of Technology, Hangzhou, Zhejiang 310014, China

^b Beijing National Laboratory for Molecular Sciences, New Cornerstone Science Laboratory, College of Chemistry and Molecular Engineering, Peking University, Beijing, China

^c Key Laboratory of Biomass Chemical Engineering of Ministry of Education, College of Chemical and Biological Engineering, Zhejiang University, Hangzhou 310027, China

^d School of Physical Sciences and CAS Key Laboratory of Vacuum Physics, University of Chinese Academy of Sciences, Beijing 100049, China

^e CAS Center for Excellence in Topological Quantum Computation, University of Chinese Academy of Sciences, Beijing 100049, China

^f Zhejiang Carbon Neutral Innovation Institute, Huzhou, Zhejiang 313200, China



ARTICLE INFO

Keywords:

CO₂ hydrogenation
Low-temperature methanol synthesis
Cu-based inverse catalyst
ZrZnO_x mixed nano-oxides
In situ DRIFTS

ABSTRACT

Hydrogenation of CO₂ into methanol at low-temperature on Cu-based catalysts is of great significance, but remains challenging to enhance activity. In this paper, we report an inverse catalyst constructed with nano-ZrZnO_x supported on Cu particles with outstanding methanol synthesis performance at 220 °C, two times higher than that of commercial Cu/ZnO/Al₂O₃ catalysts under the same conditions. Detailed structure characterization and performance evaluation demonstrate that the ZrZnO_x mixed oxide serves as the most active oxide-metal interface site for CO₂ hydrogenation. The ZrZnO_x/Cu inverse catalyst increases the weak and medium CO₂ adsorption sites which are further demonstrated responsible to the methanol productivity. *In situ* DRIFTS studies reveal that the inverse interface accelerates the reduction of asymmetric formate intermediates and prevents the generation of CO. The combination of enhanced CO₂ activation capability and accelerated hydrogenation rate of intermediates over the ZrZnO_x/Cu inverse catalyst probably contribute to the remarkable methanol synthesis performance from CO₂.

1. Introduction

The conversion of CO₂ and hydrogen produced with renewable energy into green methanol, a potential hydrogen carrier [1–4] or valued chemical feed stocks [5–7], is considered as a promising way to mitigate the negative effects of excessive CO₂ emissions [8–10]. Compared to conventional methanol synthesis based on CO hydrogenation, the hydrogenation of CO₂ is more challenging due to the lower thermodynamic advantage. Furthermore, the reaction pathway for CO₂ hydrogenation also introduces additional kinetic barriers. Formate, an important

intermediate in CO₂ hydrogenation, has been recognized as an over stabilized intermediate on most Cu/oxide catalysts, which requires higher temperatures to convert [11–14]. However, the reverse water gas shift (RWGS) reaction catalyzed by Cu-based catalysts strongly limits the selectivity of methanol at such condition [15–17]. As a result, the trade-off between catalytic activity and selectivity is one of the major challenges for conventional copper/oxide catalysts.

To achieve efficient methanol synthesis at low temperature, bypassing the conventional formate intermediate via a new reaction pathway or altering the adsorption configuration of stable formate to

* Corresponding author at: School of Physical Sciences and CAS Key Laboratory of Vacuum Physics, University of Chinese Academy of Sciences, Beijing 100049, China.

** Corresponding author.

*** Corresponding author: Institute of Industrial Catalysis, State Key Laboratory of Green Chemistry Synthesis Technology, College of Chemical Engineering, Zhejiang University of Technology, Hangzhou, Zhejiang 310014, China.

E-mail addresses: wuzhou@ucas.ac.cn (W. Zhou), dma@pku.edu.cn (D. Ma), linll@zjut.edu.cn (L. Lin).

¹ These authors contributed equally.

lower conversion barrier is highly desirable [18–20]. Significant effort has been paid in the development of novel catalytic materials. For example, the use of Mo-based materials was reported to change the activation mode of CO₂. On MoP with a large lattice constant, strong bonding of bidentate formate was less favorable than monodentate formate bonding [21]. Also, dissociation of CO₂ into CO* and further hydrogenation to methanol instead of a formate intermediate route at the double sulfur vacancies at the MoS₂ edge sites was reported to be the main reason for the superior performance of MoS₂ in methanol catalysis [22]. In terms of the conventional Cu-oxide system, it has been demonstrated that reshaping the interface structure can also be an effective strategy [23]. Inverse catalysts constructed by immobilizing ZrO₂ or ZnO nano-islands on a metallic Cu support (ZrO₂/Cu [20], ZnO/Cu [24] inverse catalyst) are preferential to form unique asymmetrically coordinated formate at the inverse interface, which is more active for hydrogenation at low temperature.

Furthermore, early studies also found the migration of H* on the catalysts is the rate-determining step of CO₂ hydrogenation to methanol over Cu/ZnO/Al₂O₃, the Pd/ZnO, and the ZnZrO_x catalysts (based on the apparent kinetic order estimated to 0.5). The strongly adsorbed CO₂ on the oxide support generally inhibits the migration of H [25]. In comparison, the inverse configuration has the continues metal phase, which could effectively promote the hydrogen spillover and the hydrogenation ability of the active intermediates. Therefore, the nano-oxide/metal inverse catalysts are highly promising catalysts for methanol synthesis from CO₂ hydrogenation at low temperature. However, there is still much work to be done to exploit the potential of the inverse catalysts [26,27]. It is well known that mixed oxide systems (In-Zr [28], Zn-Zr [29], Ga-Zr [30] and Ce-Zr [31], etc.) are much more active for CO₂ activation. Combining the special CO₂ activation behaviors of mixed oxide nanoparticles with the enhanced hydrogen activation and spillover advantages of a continuous metallic Cu particle to construct a novel inverse catalyst (mixed oxide NPs/Cu) may provide a potential way to further improve low-temperature catalytic performance in the synthesis of methanol.

Herein, we report a novel nano-ZrZnO_x/Cu inverse catalyst, composed of ZrZnO_x mixed oxide nanoparticles on a metallic Cu support, exhibits a remarkable low-temperature methanol formation rate and selectivity. The methanol formation rate of optimized ZrZnO_x/Cu inverse catalyst is more than two times higher than the commercial Cu/ZnO/Al₂O₃ catalyst at each measured space velocity from 12,000 to 144,000 mL/g_{cat}/h at 220 °C under the same reaction condition. Significantly, the performance of the ZrZnO_x/Cu inverse catalyst is also improved than that of ZrO₂/Cu and ZnO/Cu inverse catalysts. The over stabilized CO₂ adsorption sites are dramatically eliminated over the ZrZnO_x/Cu inverse catalyst according to CO₂-TPD. More importantly, the formation of ZrZnO_x mixed oxide significantly improve the density of weak and medium CO₂ adsorption sites, which is demonstrated to display a positive linear correlation with the methanol productivity. Furthermore, the intermediates formed are more active to be converted on the inverse ZrZnO_x-Cu configuration at low temperature based on the *in situ* DRIFTS characterization. The combination of enhanced CO₂ activation and hydrogenation ability over the ZrZnO_x/Cu inverse catalyst are probably the main reason for highly active methanol synthesis at low temperature.

2. Experimental

2.1. Catalyst preparation

2.1.1. Materials

The Cu(NO₃)₂·3 H₂O (99 wt% purity), Zr(NO₃)₄·5 H₂O (99 wt% purity), Zn(NO₃)₂·6 H₂O (99 wt% purity) were purchased from Sino-pharm Chemical Reagent Co., Ltd. The Oxalic Acid (99 wt% purity) were purchased from Aladdin Co., Ltd. The commercial Cu/ZnO/Al₂O₃ for methanol synthesis (the Cu, Zn and Al contents are 55, 31 and 14 mol%,

respectively) was purchased from Alfa Aesar).

2.1.2. Synthesis of ZrMO_x/Cu inverse catalysts

The ZrMO_x/Cu inverse catalysts (M=Zn, In, Ga, Ce, Mn, La, and mol_M%>50) were synthesized by two-step oxalate-mediated precipitation (CP) method. Take the ZrZnO_x/Cu catalyst with molar ratio of 9:4:87 as an example. The oxalic acid was used as a precipitating agent. In a typical synthesis procedure: 0.02 mol Cu(NO₃)₂·3 H₂O was dissolved in 100 mL ethanol. The 80 mL of 0.5 M oxalic acid in ethanol solution was added dropwise to the mixed solution at a flow rate of 1 mL/min under vigorous stirring at room temperature. After 30 min reaction, co-precipitation of Zr(NO₃)₄ (0.002 mol)-Zn(NO₃)₂ (0.001 mol) mixed solution and 20 mL of 0.5 M oxalic acid in ethanol solution. After 2 h reaction the resultant solid was separated by centrifugation, followed by washing with ethanol and drying at 70 °C for 12 h. The obtained powder was calcined in the furnace at 400 °C for 3 h. The Cu, ZnO/Cu and ZrO₂/Cu were also synthesized by the same procedures, respectively.

2.1.3. Synthesis of conventional Cu/ZnO/ZrO₂ catalysts

The conventional Cu/ZnO/ZrO₂ catalysts (mol_{Cu}%≤50) were synthesized by two-step oxalate-mediated precipitation (CP) method. Taken the synthesis of conventional Cu/ZnO/ZrO₂ (Zr:Zn:Cu molar ratio=30:20:50) catalyst as an example. First, 0.012 mol Zr(NO₃)₂·5 H₂O and 0.008 mol Zn(NO₃)₂·6 H₂O were dissolved in 100 mL ethanol. Then, 128 mL oxalic acid in ethanol solution (0.5 M) was added dropwise to the Zr(NO₃)₄-Zn(NO₃)₂ mixed solution under vigorous stirring at room temperature. After 30 min reaction, Cu(NO₃)₂·3 H₂O (0.02 mol) and 80 mL oxalic acid dissolved in ethanol solution (0.5 M) separately were added dropwise simultaneously into solution I. After 4 h reaction, the resultant solid was separated by centrifugation, followed by washing with ethanol and drying at 60 °C for 12 h. Finally, the obtained powder was calcined in the furnace at 400 °C. The Cu/ZnO/ZrO₂ (Zr:Zn:Cu molar ratio=87:4:9) were also synthesized by the same procedures.

2.2. Characterization

X-ray diffraction (XRD) patterns were recorded with a PANalytical X'Pert PRO powder diffractometer using Cu K α radiation ($\lambda = 0.1541$ nm). The working voltage was 40 kV and the working current was 40 mA. The patterns were collected with a 2 θ range from 10° to 80° at a step of 0.0167°. The average crystallite sizes of the samples were calculated with the Scherrer equation based on the strongest h k l (111) diffraction peak of CuO.

N₂ physisorption was performed on a Micromeritics ASAP-2010 instrument. The samples were first degassed in vacuum at 120 °C for 12 h before the measurement. The specific surface area and pore size distribution were calculated by using the Brunauer-Emmett-Teller (BET) method and Barrett Joyner-Halenda (BJH) desorption branch, respectively.

The metallic copper surface area (S_{Cu}) was measured using N₂O decomposition method. The catalyst (50 mg) was first reduced with 5% H₂/Ar (30 mL/min) at 300 °C for 2 h followed by purging with Ar (30 mL/min) for 30 min and cooling to 60 °C. Then, a flow of 10% N₂O/He (30 mL/min) gas was fed into the reactor for 1 h. TPR measurement was subsequently performed under a 10% H₂/Ar flow (30 mL/min) to 300 °C with a ramp rate of 10 °C/min. The copper surface area was calculated on base of Eq.1 by assuming that the copper crystallites are spherical. The amount of hydrogen consumption in first TPR was denoted as X and the second TPR was denoted as Y.

$$S_{Cu} = \frac{2 \cdot Y \cdot N_{av} \cdot \omega_{Cu}}{(x \cdot M_{Cu} \cdot 1.47 \cdot 10^{19})} (m^2 / g) \quad (1)$$

where N_{av} = the Avogadro constant, M_{Cu} = relative atomic mass (63.456 g/mol), 1.4 × 10¹⁹ derives from normalizing the average

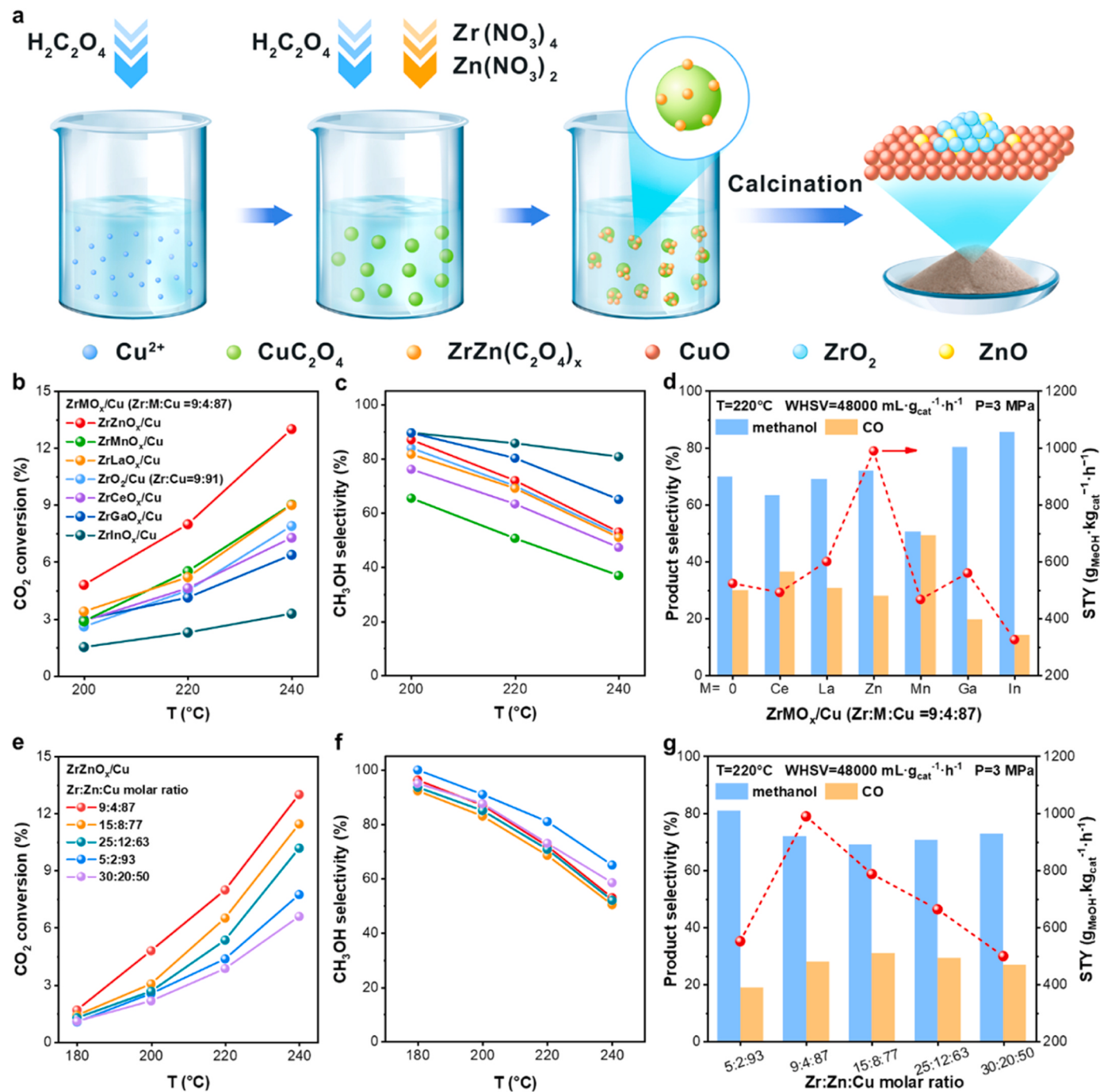


Fig. 1. Catalytic performance in the synthesis of methanol from CO_2 hydrogenation over inverse catalysts. (a) Schematic illustration of the preparation of inverse catalysts; (b) CO_2 conversion and (c) CH_3OH selectivity of ZrMO_x/Cu inverse catalysts ($M=\text{Zn, In, Ga, Ce, Mn, La, Zr}$; M:Cu molar ratio is 9:4:87); (d) comparison of product selectivity and $\text{STY}_{\text{methanol}}$ for the ZrMO_x/Cu (Zr:M:Cu = 9:4:87) inverse catalysts at a WHSV of $48000 \text{ mL}\cdot\text{g}_{\text{cat}}^{-1}\cdot\text{h}^{-1}$ at $220 \text{ }^{\circ}\text{C}$; (e) CO_2 conversion and (f) CH_3OH selectivity profiles of different Zr:Zn:Cu molar ratio for the synthesis of methanol from CO_2 hydrogenation; (g) comparison of the product selectivity and $\text{STY}_{\text{methanol}}$ for the different Zr:Zn:Cu molar ratio catalysts at a WHSV of $48000 \text{ mL}\cdot\text{g}_{\text{cat}}^{-1}\cdot\text{h}^{-1}$ at $220 \text{ }^{\circ}\text{C}$. (The Zr:Zn:Cu = 30:20:50 is the optimized ratio of conventional Cu-based methanol synthesis catalysts [32].)

copper surface atom area of 0.0711 nm^2 (equivalent to 1.4×10^{19} copper atoms per square meter).

The crystallite size of Cu and CuO is determined by Debye-Scherrer's formula (Eq. 2). The grain size reported in the manuscript was the average of the particle sizes calculated by different crystal planes (Eq. 3).

$$D_{\theta} = \frac{K\lambda}{\beta \cos \theta} \quad (2)$$

$$D_{\text{average}} = \frac{\sum_{i=1}^N D_i}{N} \quad (3)$$

D is the particle size, K is the shape factor (0.89), λ is the X-Ray wavelength (0.15406 nm), β is the full width at half maximum. θ is the Bragg's diffraction angle obtained from 2θ value corresponds to the peak in XRD pattern.

CO_2 -temperature-programmed desorption (CO_2 -TPD) measurements

were performed using a Bel mass spectrometer. The samples were treated in 5% H₂/Ar at 300 °C for 2 h (ramping rate 5 °C/min), followed by flushing with Ar for 30 min before cooled to 50 °C. CO₂ adsorption was performed in 10% CO₂/He for 60 min, after which the samples were flushed with Ar for 40 min to remove the un-adsorbed CO₂. Then, the CO₂ desorption was performed. The heating rate was set as 10 °C/min. A mass spectrometer (Bel mass) was used to detect the desorbed CO₂.

The STEM (scanning transmission electron microscopy) analysis was conducted using Nion UltraSTEM-100 electron microscopy operated at 60 kV. The Z-contrast images were collected with an annular dark field detector in the range of 75–210 mrad with a convergence angle of 32 mrad on Nion. Electron energy-loss spectroscopy was carried out with the same experimental set-up with a probe current of about 50 pA. The samples for electron microscopy characterization were prepared by directly dropping in ethanol solvent on gold grids coated holey carbon film.

The AP-XPS measurement were carried out on a commercial SPECS AP-XPS chamber equipped with a PHOIBOS 150NAP, 1D-DLD analyzer. The ZrZnO_x/Cu (9:4:87) and ZnO/Cu (0:5:95) catalysts are conductive during AP-XPS measurement, no charge was accumulated on the surface of the catalysts. The ZrZnO_x/Cu (9:4:87) and ZnO/Cu (0:5:95) catalyst powders were pressed on a tantalum plate and then loaded into the AP-XPS chamber. The sample was first reduced with 20 mL/min 10% H₂ at 300 °C for 2 h and cooled down to room temperature. Then 2 mbar CO₂/H₂/N₂ mixture (24/72/4) were introduced into the reaction chamber. Zr 3d, Zn 2p, Cu 2p, Cu LMM, O 1 s, and C 1 s XPS regions were collected at the conditions of fresh, after reduction and after reaction gas environment for 1 h and 3 h.

Operando DRIFTS measurements were carried out using an FTIR spectrometer of Bruker Vertex 80 equipped with a Harrick cell and an MCT detector. The spectra were expressed in units of Kubelka-Munk (K-M). The ZrZnO_x/Cu (9:4:87) and Cu/ZnO/ZrO₂ (Zr:Zn:Cu=87:4:9) catalysts were first pretreated in diluted 10% H₂/Ar gas flow at 300 °C for 2 h, then cooled down to 220 °C. The background was collected in the Ar flow at 30 mL/min, later, the gas flow was changed to 75% H₂/25% CO₂ (30 mL·min⁻¹, 0.1 MPa) and the spectra were collected simultaneously for 75 min, taking as reaction stage. The inlet gas was changed to 15% H₂/Ar at 220 °C for another 50 min, which is referred as hydrogenation stage. After that, the samples were tested under different pressure conditions (1 MPa or 3 MPa), the evolutions of functional groups on samples surfaces were recorded by FTIR spectrometer.

The H₂-D₂ exchange experiment was conducted in a fixed-bed flow reactor. The ZrZnO_x/Cu (9:4:87) and Cu/ZnO/ZrO₂ (Zr:Zn:Cu=87:4:9) catalysts (20 mg catalysts diluted with 80 mg SiO₂) were first pretreated in diluted 5% H₂/Ar gas flow at 300 °C for 2 h. After cooling down to room temperature, the gas was switched to 5%vol D₂/5%vol H₂/Ar (flow rate = 10 mL/min) and waiting for the signals to be stable. The H-D exchange was temperature-programmed with a rising 5 °C/min from 30 °C to 300 °C. Mass spectrometry (OMNI Star™ Gas Analysis System) was used to analyze the signal of *m/z* = 2 (H₂), 3 (HD), 4 (D₂), 18 (H₂O), 40 (Ar). All the signal is normalized by *m/z* = 40 to eliminate the variations of response in mass spectrometry.

The Electron Paramagnetic Resonance (EPR) experiments were carried out on Bruker EMX plus EPR Spectrometer under a condition of liquid nitrogen temperature 100 K, microwave frequency 9.39 GHz and microwave power 2.00 mW.

2.3. Catalyst evaluation

The performance evaluation for CO₂ hydrogenation to methanol was performed in a high-pressure fixed-bed reactor. 50 mg catalyst was diluted with 200 mg quartz sand, and then packed into the stainless-steel tubular reactor. Prior to the catalytic measurements, the catalyst was reduced in a stream of 5% H₂/N₂ at 300 °C for 2 h under atmospheric pressure. Then, the temperature was cooled to 200 °C, and the reductive gas was replaced by the reaction gas of CO₂: H₂: N₂ at a ratio of

24:72:4. The N₂ was taken as internal standard. The reaction was performed with a pressure of 3.0 MPa. The catalytic activity test was taken at 180, 200, 220 and 240 °C. The reactants and products flowing out in the reactors were analyzed by an online gas chromatographer (GC-8860, Agilent) equipped with a TCD and a flame ionization detector (FID). The CO₂ conversion and CH₃OH selectivity were obtained from the GC data. The conversion, selectivity, and space time yield (STY) were defined in the following equation:

$$X(CO_2)\% = \frac{F \bullet C_{in}(CO_2) - F \bullet \frac{A_{N_2in}}{A_{N_2out}} C_{out}(CO_2)}{F \bullet C_{in}(CO_2)} \quad (4)$$

$$S(CH_3OH)\% = \frac{n(CH_3OH)}{\sum n(products)} \quad (5)$$

$$S(CO)\% = \frac{n(CO)}{\sum n(products)} \quad (6)$$

$$STY(CH_3OH)(g_{CH_3OH} \bullet kg_{cat}^{-1} \bullet h^{-1}) = \frac{n_{in}(CO_2) \bullet X(CO_2) \bullet S(CH_3OH) \bullet 32 \bullet 60}{22.4 \bullet m_{cat}} \quad (7)$$

$$Carbon \ balance\% = \frac{\sum n(products)}{n_{in}(CO_2) - n_{out}(CO_2)}$$

The carbon balances in the experiments are between 95% to 101%.

3. Result and discussion

3.1. Catalytic performance evaluation

Inverse catalysts are synthesized by using a two-step oxalate-mediated precipitation (CP) method (Fig. 1a) [33,34]. After calcination and reduction, the catalysts are denoted as ZrMO_x/Cu (Zr:M:Cu molar ratio is a:b:c, M=Zn, In, Ga, Ce, Mn, La). Other reference binary ZnO/Cu and ZrO₂/Cu catalysts are synthesized using the same method [33]. It has been confirmed that the ZrO₂/Cu inverse catalyst showed the highest STY_{methanol} when Zr:Cu molar ratio is 1:10 in our previous work [33]. So the optimal molar ratio of Zr:M:Cu of the ZrMO_x/Cu inverse catalysts is firstly explored when Zr:Cu closes to 1:10, and it is found that the catalyst shows the best performance of methanol synthesis with the Zr:Zn:Cu molar ratio is 9:4:87 (Fig. S1, and the actual percentage of elements in the total weight is shown in Table S1), that is, the oxide loading is ~13 mol%. The catalytic performance of ZrZnO_x/Cu (Zr:Zn:Cu=9:4:87) inverse catalyst is further evaluated together with other ZrMO_x/Cu inverse catalysts (Zr:M:Cu=9:4:87) as shown in Fig. 1b-d. Among all catalysts, the ZrZnO_x/Cu (Zr:Zn:Cu=9:4:87) inverse catalyst shows the highest CO₂ conversion activity as a function of temperature from 200 to 240 °C at a WHSV of 48000 mL·g_{cat}⁻¹·h⁻¹. More importantly, the ZrZnO_x/Cu (Zr:Zn:Cu=9:4:87) inverse catalyst maintains a comparable methanol selectivity with other counterparts at each temperature even though it enables the highest CO₂ conversion (Fig. 1b-c). The STY_{methanol} of ZrZnO_x/Cu (Zr:Zn:Cu=9:4:87) inverse catalyst reaches 990 g_{MeOH}·kg_{cat}⁻¹·h⁻¹ (CO₂ conversion=8.4% and methanol selectivity=70%) at 220 °C, 1.7 and 1.9 times higher than ZrLaO_x/Cu (Zr:La:Cu=9:4:87) and ZrO₂/Cu (Zr:Cu=9:91) catalysts (Fig. 1d). Some prepared mixed oxide composites, like ZrInO_x and ZrMnO_x, show a negative effect on CO₂ hydrogenation compared with ZrO₂/Cu. Furthermore, keep the molar ratio of Zr:Zn close to 9:4 and change molar ratio of ZrZnO_x/Cu (the accurate content is shown in Table S2), the catalytic performance gradually decreases when the percentage of oxide exceeds 13 mol%, indicating that the coverage of nano-ZrZnO_x at 13 mol% is the optimal composition of the inverse catalysts for the hydrogenation of CO₂ to methanol (Fig. 1e-f). The STY_{methanol} of 13 mol% ZrZnO_x/Cu (9:4:87) inverse catalyst is also 2.1 times higher than the conventional Cu/ZnO/ZrO₂ catalysts (the optimized molar ratio of Zr:

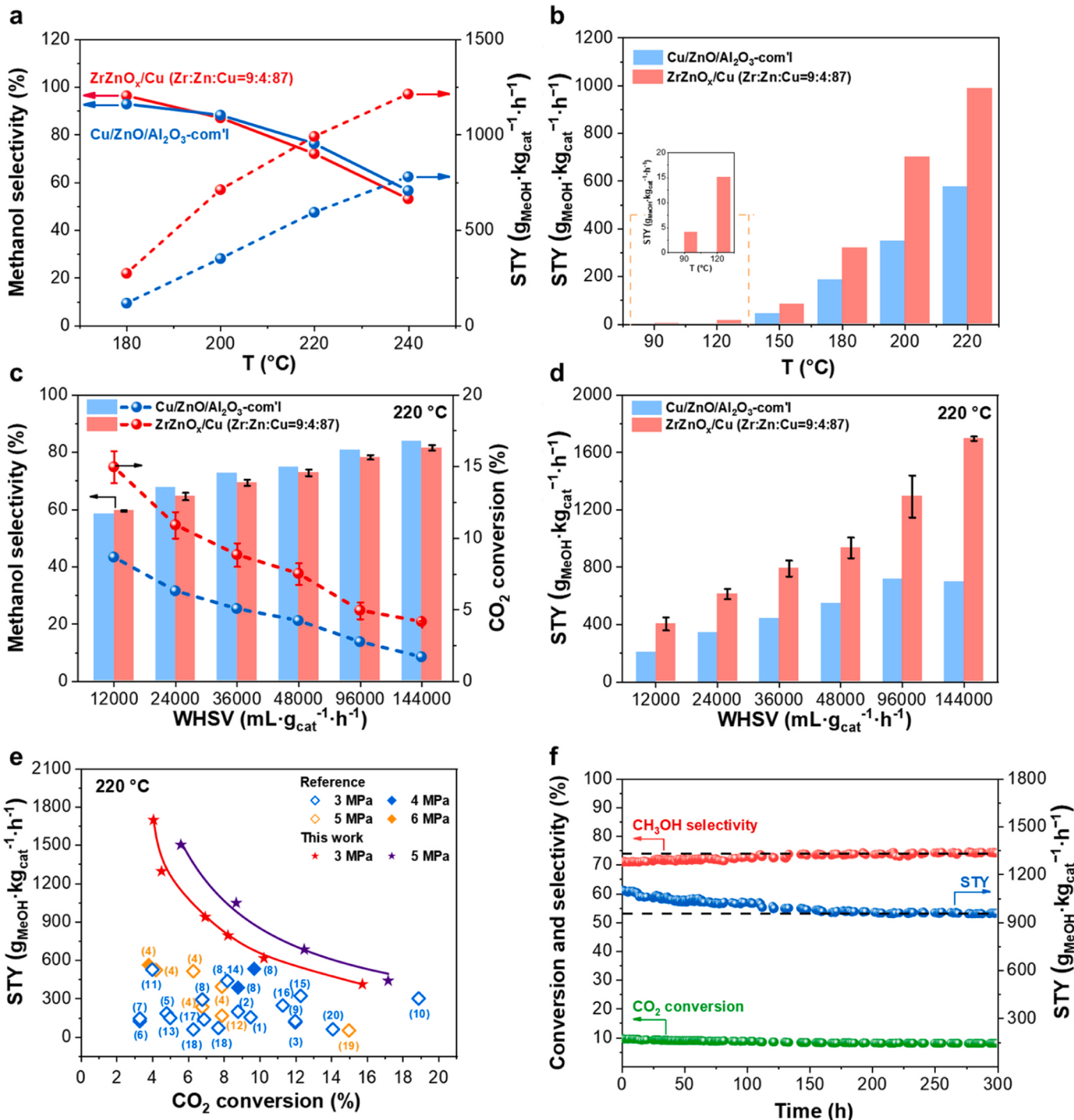


Fig. 2. The comparison of methanol production activity of ZrZnO_x/Cu inverse catalyst with Cu-based reference catalysts. (a) comparison of CO₂ hydrogenation activity and methanol selectivity between the ZrZnO_x/Cu inverse catalyst and Cu/ZnO/Al₂O₃-com'l catalyst (55 mol% Cu, purchased from Alfa Aesar) (Reaction conditions: CO₂:H₂:N₂ = 24:72:4, WHSV = 48000 mL·g_{cat}⁻¹·h⁻¹, P = 3.0 MPa); (b) the STY_{methanol} for the ZrZnO_x/Cu and Cu/ZnO/Al₂O₃ commercial catalysts from 90 to 220 °C (Reaction conditions: CO₂:H₂:N₂ = 24:72:4, WHSV = 48000 mL·g_{cat}⁻¹·h⁻¹, P = 3.0 MPa); (c) CO₂ conversion and methanol selectivity, and (d) STY_{methanol} of ZrZnO_x/Cu inverse catalyst and Cu/ZnO/Al₂O₃-com'l as a function of WHSV; (e) the catalytic activity of the ZrZnO_x/Cu inverse catalyst compared with catalysts reported in literature in CO₂-STY_{methanol} conversion diagram. The numbers are referred to catalysts as following: (1) Cu/ZnO/ZrO₂ [35], (2) Cu-MoC₂/MCM-41 [36], (3) Cu/ZnO/ZrO₂ [37], (4) FL-MoS₂, Cu/Zn/Al₂O₃ [22], (5) CuAl/CeO₂ [38], (6) Cu-Ni/CeO₂ [39], (7) Cu/La₂O₃CO₃ [40], (8) M-CZZ, C-CZZ [32], (9) CAZ-1.25 [41], (10) macroporous Cu/ZnO/ZrO₂ [42], (11) ZrO₂/Cu-0.1 [33], (12) Cu-ZnO-ZrO₂ [43], (13) CM-300 [44], (14) 12% Cu-ZrO₂ [45], (15) 4CZA-AE [46], (16) 8-CZA-S [47], (17) CuIn-350 [48], (18) 0.5Ca5Pd5ZnCeO₂, 5Pd5ZnCO₂ [49], (19) CuZnAl-4 [50], (20) 30Cu/Zn/ms-SiO₂ [51]; (f) the long-term stability of the ZrZnO_x/Cu inverse catalyst. (Reaction conditions: CO₂:H₂:N₂ = 24:72:4, WHSV = 48000 mL·g_{cat}⁻¹·h⁻¹, T = 220 °C, P = 3.0 MPa).

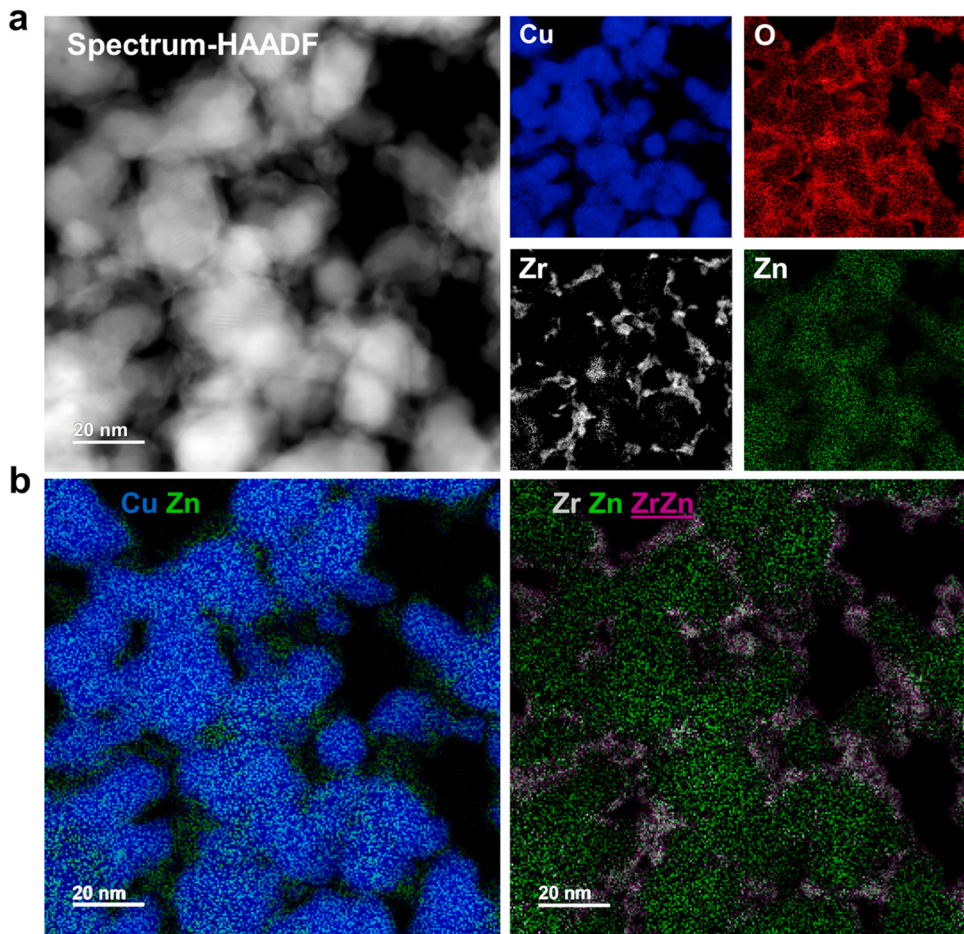


Fig. 3. Electron microscopy characterization of spent ZrZnO_x/Cu inverse catalyst. (a) STEM-HAADF imaging and corresponding EELS elemental mappings of Cu, Zr and Zn; (b) the superimposed STEM-EELS elemental mappings of Zn (green) and Cu (blue), and Zr (gray), Zn (green), purple is a mixed color of gray and green when putting the EELS mapping images of Zn (green) and Zr (gray) together.

Zn:Cu is 30:20:50 reported in the literature [32], Fig. 1g).

The low temperature catalytic performance of ZrZnO_x/Cu (9:4:87) is also compared with that of the commercial $\text{Cu}/\text{ZnO}/\text{Al}_2\text{O}_3$ (denoted as $\text{Cu}/\text{Zn}/\text{Al}_2\text{O}_3\text{-com}'1$, 55 mol% Cu, purchased from Alfa Aesar) under the same reaction condition (Fig. 2a). The space time yield of the ZrZnO_x/Cu inverse catalyst at 200 °C reached $710 \text{ gMeOH}\cdot\text{kg}_{\text{cat}}^{-1}\cdot\text{h}^{-1}$, which equals to that of $\text{Cu}/\text{ZnO}/\text{Al}_2\text{O}_3\text{-com}'1$ at 240 °C. While the activity of ZrZnO_x/Cu inverse catalyst at 240 °C is $1213 \text{ gMeOH}\cdot\text{kg}_{\text{cat}}^{-1}\cdot\text{h}^{-1}$, nearly 1.5 times higher than that of $\text{Cu}/\text{ZnO}/\text{Al}_2\text{O}_3\text{-com}'1$ catalyst. Furthermore, methanol appears in the product of CO_2 hydrogenation reaction over ZrZnO_x/Cu inverse catalyst at only 90 °C, ~30 °C lower than that of $\text{Cu}/\text{ZnO}/\text{Al}_2\text{O}_3\text{-com}'1$ catalyst (Fig. 2b), which further confirms the remarkable low-temperature activity of the inverse catalyst. CO_2 conversion and methanol selectivity as a function of space velocities are measured on ZrZnO_x/Cu inverse catalyst and $\text{Cu}/\text{ZnO}/\text{Al}_2\text{O}_3\text{-comm}'1$ catalyst to obtain the intrinsic methanol formation rate (Fig. 2c-d). Even though CO_2 conversion of the ZrZnO_x/Cu inverse catalyst is twice higher than that of $\text{Cu}/\text{ZnO}/\text{Al}_2\text{O}_3\text{-com}'1$, the selectivity of methanol on the inverse catalyst remains similar with that of the commercial catalyst. At WHSV of $144,000 \text{ mL}\cdot\text{g}_{\text{cat}}^{-1}\cdot\text{h}^{-1}$, a remarkable methanol formation rate of $1696 \text{ gMeOH}\cdot\text{kg}_{\text{cat}}^{-1}\cdot\text{h}^{-1}$ is achieved on ZrZnO_x/Cu inverse catalyst, 2.4 times higher than the $\text{Cu}/\text{ZnO}/\text{Al}_2\text{O}_3\text{-com}'1$ catalyst (Fig. 2d). In addition, the STY of methanol over the ZrZnO_x/Cu inverse catalyst at 220 °C as a function of CO_2 conversion is presented in Fig. 2e and Table S3 together with other state-of-the-art catalysts. It demonstrates that ZrZnO_x/Cu inverse catalyst in this work exhibits much higher methanol production activity than other oxide-supported catalysts of methanol

synthesis at each similar CO_2 conversion at the low temperature of 220 °C, indicating that the ZrZnO_x/Cu inverse catalyst is probably among the most competitive Cu-based catalysts for the low-temperature methanol synthesis from CO_2 . Also, the stability of the ZrZnO_x/Cu inverse catalyst is evaluated at 220 °C with WHSV of $48,000 \text{ mL}\cdot\text{g}_{\text{cat}}^{-1}\cdot\text{h}^{-1}$ (Fig. 2f). The STY_{methanol} approaches stable after 120 h time on stream and remains unchanged in the next 180 h. The Cu particle sizes of the fresh and spent catalysts are ~14.0 nm and 17.9 nm, respectively (based on XRD results, Fig. S2), suggesting the Cu support is robust without significantly aggregation in the CO_2 hydrogenation conditions. The ZrZnO_x oxide particles are well dispersed on CuO/Cu support before and after reaction, indicating the oxide particles are highly stable under reaction condition.

3.2. Active sites identification

High angle angular dark field scanning transmission electron microscopy (HAADF-STEM) imaging [52] and electron energy loss spectroscopy (EELS) elemental mapping are applied to explore the structure of the spent ZrZnO_x/Cu inverse catalyst to identify the active sites responsible for the enhanced performance (Fig. 3). EELS elemental mappings show the spatial distributions of the Zr, Zn and Cu elements in the ZrZnO_x/Cu inverse catalyst. As shown in Fig. 3a, the elemental mappings of Zr and Cu indicate that the size of oxides loaded on the Cu particles is 2–5 nm. Zn element displays a dual distribution on both Cu support and the oxide particles. The detailed analysis of spatial-resolved EELS spectra highlights the regions of containing only Zr (gray), Zn (green) and coexisting Zr and Zn (purple) (Fig. 3b) and the results prove

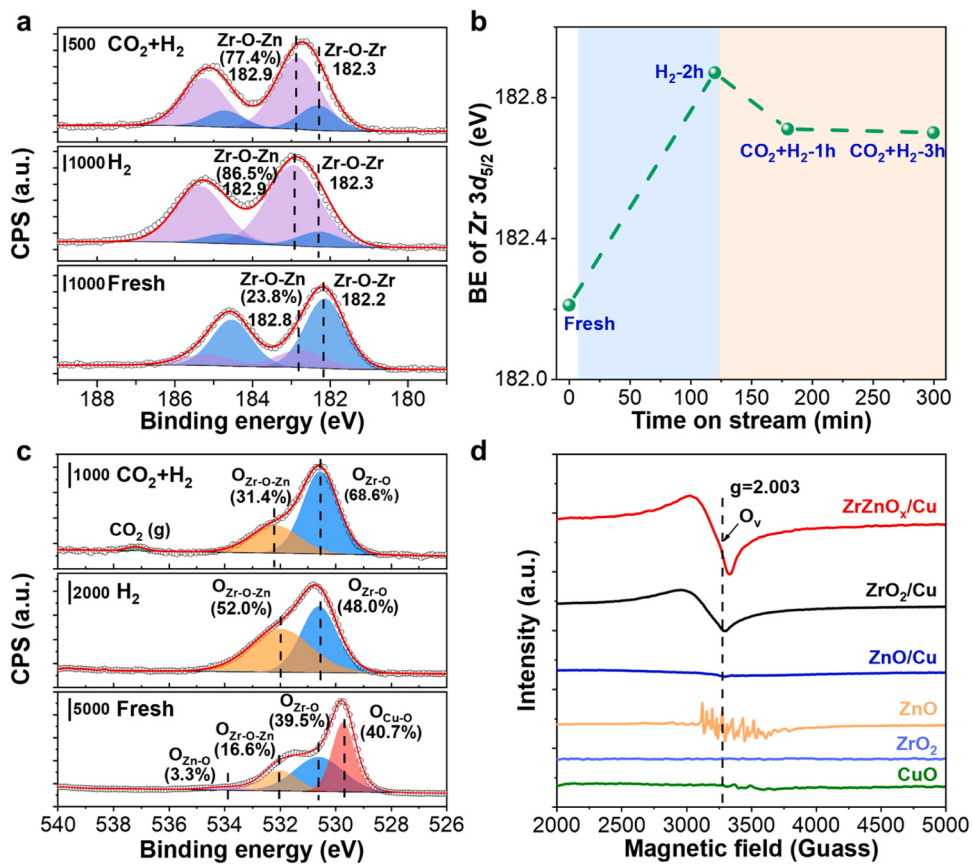


Fig. 4. The XPS profiles of (a) Zr 3d region, (b) the variation of binding energy of Zr 3d as a function of time on different streams during AP-XPS measurement and (c) O 1 s region of the ZrZnO_x/Cu inverse catalyst; (d) EPR spectra of CuO, ZrO₂, ZnO, ZnO/Cu, ZrO₂/Cu and ZrZnO_x/Cu catalysts.

supported nano-oxides is composed with Zr-Zn mixed oxide and ZrO₂.

Ambient-pressure XPS (AP-XPS) is used to study the chemical properties and surface composition of ZrZnO_x/Cu inverse catalyst (Fig. 4 and Figs. S3–4). The Cu LMM Auger electron spectroscopy suggests that Cu is fully reduced to Cu (0) (K.E.=918.4 eV) after reduction [53,54], and it remains metallic in the CO₂-H₂ atmosphere (Fig. S3). It is worth noting that an unusual shift in binding energy of Zr 3d is observed from 182.2 eV (conventional Zr (IV) in ZrO₂) to 182.8 eV after reduction (Fig. 4a) [55]. After exposure to the mixture of CO₂-H₂ conditions, the binding energy of Zr slightly shifted backward to 182.6 eV, which is still more positive (~0.4 eV) than that of the reduced fresh catalyst. The peak deconvolution suggests a new Zr-O-Zn linkage centered at 182.8 eV is the major surface species under reducing atmosphere (86.5%) after reduction, which pointing to the formation of ZrZnO_x mixed oxide nanoparticles on the inverse catalyst [30]. Although the intensity of Zr-O-Zn linkage decreases after exposing to CO₂-H₂ mixture, the percentage of this component is constant in the reaction atmosphere (Fig. 4b). In addition, the spectroscopy of O 1 s was analyzed and shown in Fig. 4c, the O 1 s at binding energy of 532.0 eV is related with Zr-O-Zn species [30], which is higher than that of Zr-O in ZrO₂. Also, the percentage of Zr-O-Zn is increased from 16.6% to 52.0% after reduction, which is in good agreement with the deconvolution of Zr 3d spectra.

The EPR experiments are further performed to investigate the oxygen vacancies in the catalysts (Fig. 4d) [56]. The ZrZnO_x/Cu exhibited the largest amount of oxygen vacancies ($g=2.003$) [57,58], followed by ZrO₂/Cu. And, almost no signals related to the oxygen vacancies is observed on ZnO/Cu. As a result, it can be confirmed that the ZrO₂ nano oxide particles contains rich structure defects. The introduction of Zn enhances the oxygen vacancies of ZrO₂ which serves as a good evidence for the formation of mixed oxide species.

The most active interface in the inverse catalyst (ZnO/Cu, ZrO₂/Cu

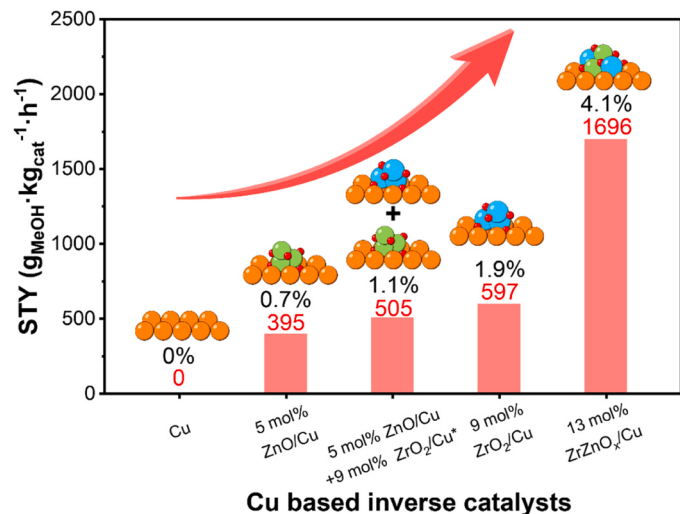


Fig. 5. STY of methanol over varied Cu-based inverse catalysts in CO₂ hydrogenation. * refer to physically mixed catalysts. (Reaction conditions: CO₂:H₂:N₂ = 24:72:4, P = 3.0 MPa, WHSV=144000 mL·g_{cat}⁻¹·h⁻¹).

or ZrZnO_x/Cu) for methanol synthesis from CO₂ hydrogenation was further evaluated by comparing the catalytic performance of 4 mol% ZnO/Cu, 9 mol% ZrO₂/Cu and physical mixed catalysts of 4 mol% ZnO/Cu + 9 mol% ZrO₂/Cu catalyst at CO₂ conversion below 4% (Fig. 5). The methanol formation rates of 4 mol% ZnO/Cu inverse catalyst, 9 mol% ZrO₂/Cu and physical mixed catalysts are only 395, 597 and 505 g_{MeOH}·kg_{cat}⁻¹·h⁻¹, much lower than that of 13 mol% ZrZnO_x/Cu

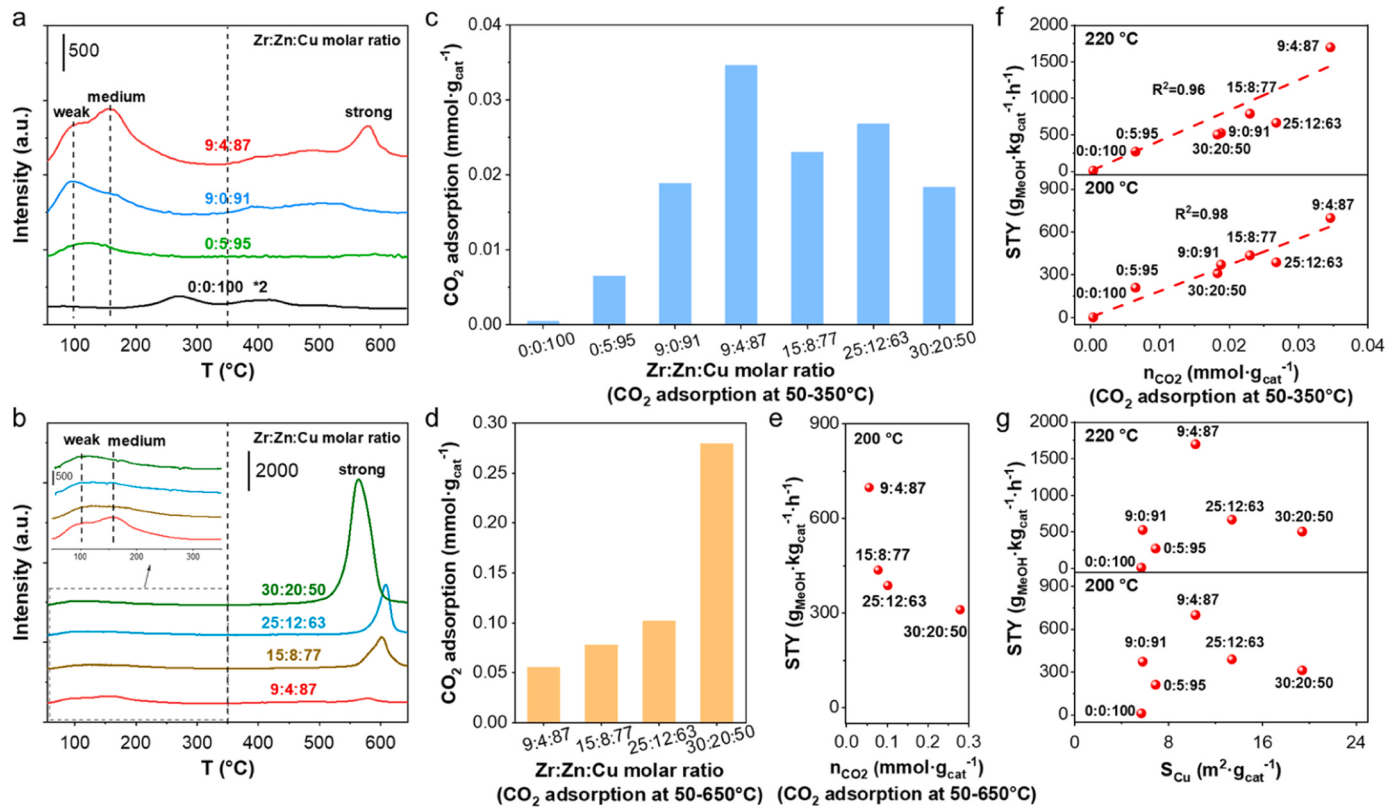


Fig. 6. Study of CO₂ adsorption site and ability to activate CO₂ of different catalysts. (a-b) The CO₂-TPD profiles in varied Cu-base catalysts; (c) the amount of weak and medium adsorbed CO₂ estimated from the CO₂-TPD profiles at the temperature of 50–350 °C, (d) the amount of adsorbed CO₂ estimated from the CO₂-TPD profiles at the temperature of 50–650 °C; (e) the correlation of the STY_{methanol} (at 200 °C) and the amount of adsorbed CO₂ at 50–650 °C; (f) the correlation of the STY_{methanol} (at 200 and 220 °C, respectively) and the amount of adsorbed CO₂ at 50–350 °C; (g) the correlation of STY_{methanol} (at 200 and 220 °C, respectively) and the exposed sites of metallic copper.

catalyst of 1696 g_{MeOH}·kg_{cat}⁻¹·h⁻¹, indicating that the existence of synergistic effect between Zn and Zr oxides and enhanced oxygen vacancies in the ZrZnO_x/Cu inverse catalyst accounting for the remarkable methanol formation rate.

3.3. The relationship between active sites and performance

To investigate the functions of ZrZnO_x mixed oxide on the catalytic performances, CO₂ temperature programmed desorption (CO₂-TPD) experiments on the ZrZnO_x catalysts with different Zr:Zn:Cu molar ratio to delve into the adsorption behavior of CO₂ on different surface sites (Fig. 6a-b and Fig. S5). As shown in Fig. S5, CO₂ adsorption is almost undetectable on bare ZnO, and the majority of CO₂ adsorption on bare ZrO₂ (bulk phase) is at high temperature of 600 °C (strong adsorption). When the oxide is loaded onto the metal Cu support, the CO₂ desorption amount per gram of oxide at 30–350 °C is 3 and 40 times higher than that on bare ZrO₂ and bare ZnO, indicating that the weak and medium adsorption of CO₂ is mainly related to the metal-oxide interface [59,60] or oxygen vacancies. It has been reported that the CO₂ adsorbed on the oxygen vacancies of reducible oxides normally desorbs at 50–350 °C [57,58]. The amount of weak and medium adsorbed CO₂ are improved on ZrZnO_x/Cu catalysts than that of ZrO₂/Cu and ZnO/Cu catalysts (Fig. 6c), which is consistent with the change of performance of methanol synthesis (Fig. 5). With the increasing loading of ZrZnO_x, the intensity of high-temperature desorption peak increases rapidly. However, the signals corresponding to the desorption of weak and medium adsorbed CO₂ do not increase proportionally. The quantification of the density of CO₂ adsorption sites (Fig. 6c-d) suggests the formation of ZrZnO_x nano-oxide on the Cu support maximizes the density of weak-medium adsorption sites of CO₂ (0.035 mmol/g_{cat}) compared with

ZrO₂/Cu (0.019 mmol/g_{cat}) and ZnO/Cu (0.007 mmol/g_{cat}) as well as conventional Cu/ZnO/ZrO₂ (Cu:Zn:Zr=50:20:30) catalyst. The reverse correlation of the high-temperature desorption peaks with the productivity of methanol (Fig. 6d and Fig. 6e) demonstrate the strongly adsorbed CO₂ are the spectator of CO₂ hydrogenation reaction. Indeed, when correlates the STY_{methanol} of ZrZnO_x/Cu catalysts with different Zr:Zn:Cu molar ratio at 200 and 220 °C with the density of weak and medium adsorption sites, two linear curves appear respectively (Fig. 6f), which strongly supports that the conversion of the reactive adsorbed CO₂ species are key factor for enhancing methanol productivity. Therefore, the 13 mol% ZrZnO_x/Cu (Zr:Zn:Cu=9:4:87) inverse catalyst which holds the highest density of reactive adsorption sites displays the highest methanol formation rate. Furthermore, the exposing surface area of metallic Cu sites are determined using N₂O selective oxidation and chemical titration. Although the molarity of Cu in inverse catalysts is much higher than conventional Cu catalysts, the exposing surface area of metallic Cu of inverse catalyst is relatively small (Fig. 6g). The lack of positive/negative correlation of Cu sites and the activity of catalysts also demonstrate the hydrogen activation (generally occurs on Cu surface) is not the crucial factors for methanol synthesis from CO₂.

DRIFTS spectroscopy is used to understand the mechanism of low-temperature CO₂ hydrogenation on the ZrZnO_x/Cu (Zr:Zn:Cu=9:4:87) inverse catalyst (Fig. 7), with the Cu/ZnO/ZrO₂ (Cu:Zn:Zr=9:4:87) catalyst as a comparison. The ZrZnO_x/Cu (Zr:Zn:Cu molar ratio =9:4:87) catalyst exhibits more than three times higher catalytic activity than conventional Cu/ZnO/ZrO₂ (Cu:Zn:Zr=9:4:87) catalyst from 200 to 240 °C (Fig. S6). And, the particle size of loaded Cu on the contrasted Cu/ZnO/ZrO₂ catalyst is approximately 2–5 nm, which can be regarded as metal-oxide interface (Fig. S7). A novel band at 1350 cm⁻¹ appears on the ZrZnO_x/Cu inverse catalyst in addition to the bands for bidentate

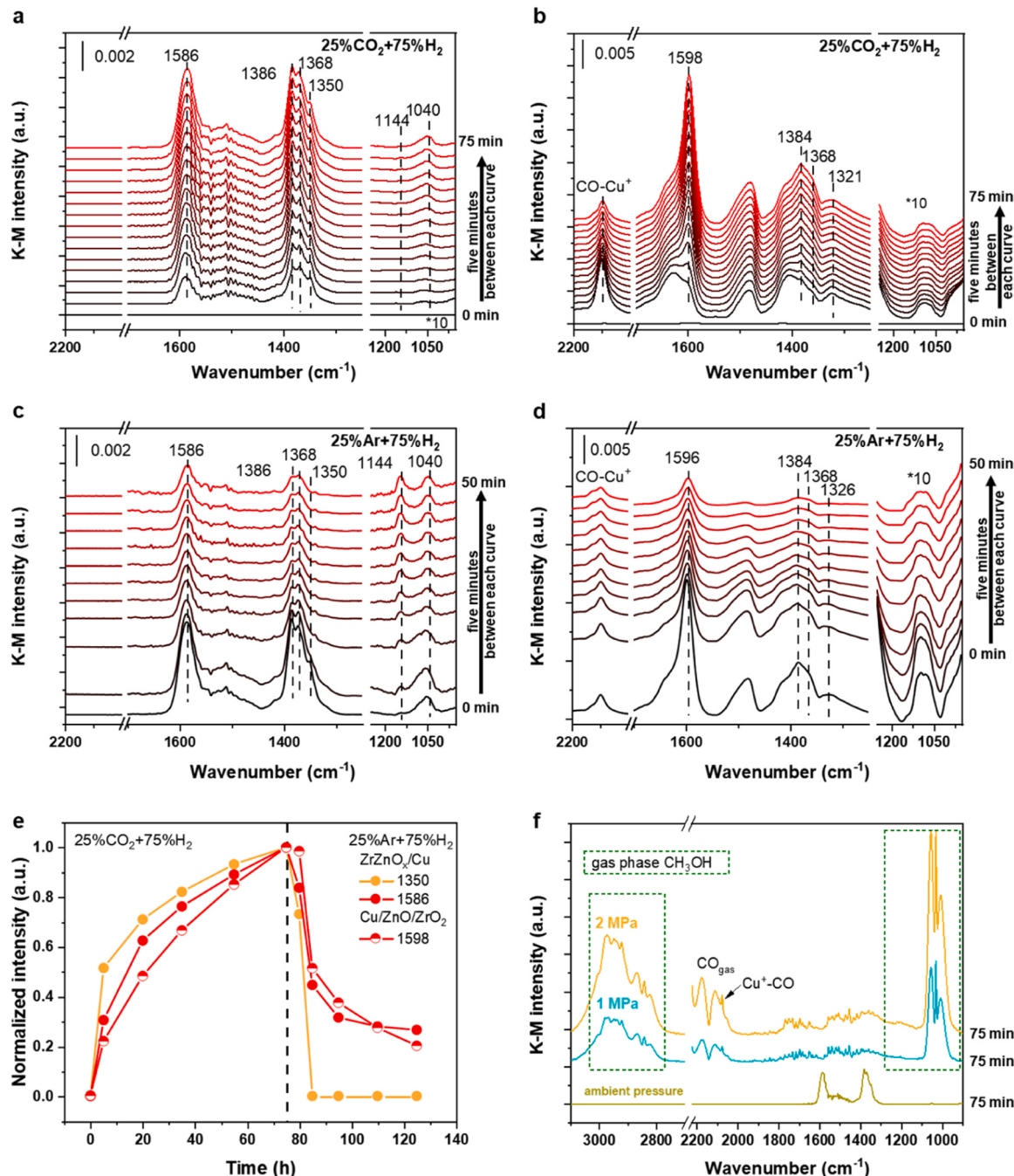


Fig. 7. Surface intermediates investigation by *in situ* DRIFTS characterization. (a-d) DRIFTS results of the ZrZnO_x/Cu inverse catalyst and contrasted Cu/ZnO/ZrO₂ catalyst in the stream of CO₂/H₂ mixture for 75 min (a-b) and, then in the stream of H₂/He for 50 min (c-d) under ambient pressure at 220 °C; (e) Normalized intensities of the typical surface species, bidentate formate (~1580 cm⁻¹ for ZrZnO_x/Cu, red solid circle; ~1598 cm⁻¹ for Cu/ZnO/ZrO₂, Red half-filled circle) and the peak of asymmetric formate intermediate HCOO-Cu (1350 cm⁻¹, orange solid circle) species versus reaction time. (f) DRIFTS results of the ZrZnO_x/Cu inverse catalyst in the stream of CO₂/H₂ mixture under 1.0 MPa and 2.0 MPa respectively at 220 °C.

formate (1580, 1380 and 1368 cm⁻¹) [15] after exposed to the reaction atmosphere, which can be attributed to asymmetrically coordinated formate at the oxide-metal inverse interface (Fig. 7a) [33,61]. In comparison, no signals for the asymmetrically coordinated formate (1350 cm⁻¹) or methoxy groups (1040 cm⁻¹) appear at the metal-oxide interface of the contrasted Cu/ZnO/ZrO₂ catalyst under the same reaction. Instead, strong peaks for bicarbonate (HCO₃⁻) appeared at 1640 and 1420 cm⁻¹, indicating that the hydrogenation of adsorbed CO₂ is slower on the Cu/ZnO/ZrO₂ catalyst (Fig. 7b). When the CO₂ in the mixture is removed, the steady state intermediates are exposed to H₂ atmosphere in order to compare the hydrogenation ability of the catalysts (Fig. 7c-d).

Meanwhile, with increasing reaction time, the intensity of formate decreases dramatically on ZrZnO_x/Cu inverse catalyst, while the band for methoxy (1050 cm⁻¹) exists with the similar intensity, it indicates that the reduction of the formate to methoxy, and methoxy hydrogenation to methanol (1144 cm⁻¹) show similar reaction rate (Fig. 7c and Fig. S8a). In contrast, the band for methoxy or methanol is hardly observed on the conventional Cu/ZnO/ZrO₂ configuration. Meanwhile, the intensity of linearly adsorbed Cu⁺-CO* (2100 cm⁻¹) is strong on the conventional Cu/ZnO/ZrO₂ interface, which may lead to the generation of byproduct CO (Fig. 7d and Fig. S8b). Quantitative analysis by tracking the intensity changes of relative intermediates was performed (Fig. 7e). Quick

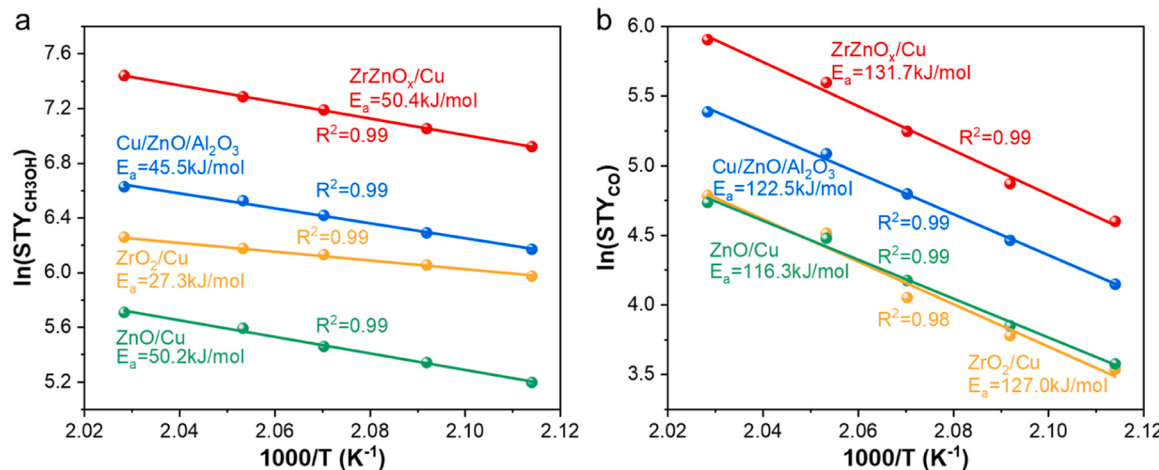


Fig. 8. Apparent activation energy measurements of ZrZnO_x/Cu , $\text{Cu}/\text{ZnO}/\text{Al}_2\text{O}_3$, ZrO_2/Cu , and ZnO/Cu catalysts. (a) methanol-based E_a ; and (b) CO-based E_a .

consumption of the band at 1350 cm^{-1} on ZrZnO_x/Cu inverse catalyst suggests that the asymmetrically coordinated formate is very reactive. Then, $\text{H}_2\text{-D}_2$ exchange experiment was performed (Fig. S9). It shows that the initial hydrogen dissociation temperatures of ZrZnO_x/Cu (Zr:Zn:Cu=9:4:87) and $\text{Cu}/\text{ZnO}/\text{ZrO}_2$ (Zr: Zn: Cu=87:4:9) are 135°C and 105°C , respectively, indicating that the dissociation ability of hydrogen is not the main factor affecting the performance between inverse catalyst and traditional catalyst. In general, the asymmetrically coordinated formate is probably the main reason for the superior hydrogenation capability of ZrZnO_x/Cu inverse catalyst. Furthermore, when the reactants were changed to high-pressure $\text{CO}_2\text{-H}_2$ mixture (1 and 2 MPa) over ZrZnO_x/Cu inverse catalyst, the signals for oxygenated intermediates on the ZrZnO_x/Cu inverse catalyst almost disappeared. Simultaneously, a large amount of gas-phase CH_3OH appear by peaks at $3000\text{--}2800$ and $1100\text{--}1000 \text{ cm}^{-1}$, suggesting that there are almost no over-stable oxygenates in the reaction network for the CO_2 hydrogenation reaction over the ZrZnO_x/Cu inverse catalyst (Fig. 7f) [62].

The apparent activation energy of ZrZnO_x/Cu , commercial $\text{Cu}/\text{ZnO}/\text{Al}_2\text{O}_3$, ZnO/Cu and ZrO_2/Cu catalysts were also measured (Fig. 8). Except for ZrO_2/Cu catalyst, the E_a of the other three catalysts are similar for methanol synthesis, but ZrZnO_x/Cu catalyst exhibits the largest E_a for RWGS reaction (calculated based on the productivity of CO), which maybe the main reason for the better methanol selectivity of ZrZnO_x/Cu . Actually, even though the ZrO_2/Cu shows the lowest E_a for methanol synthesis, the relatively low density of active sites limits the catalytic performance. In summary, it can be implied that the Zn species in the inverse ZrZnO_x/Cu catalysts mainly enhances the density of active sites and simultaneously suppressed the undesirable RWGS side reactions.

4. Conclusions

The inverse catalyst constructed with ZrZnO_x mixed oxide particles on a Cu support exhibits an extraordinary methanol formation activity of $990 \text{ g}_{\text{MeOH}} \text{ kg}_{\text{cat}} \text{ h}^{-1}$ (Conv. $\text{CO}_2=8.4\%$, WHSV=48,000 mL/g_{cat}/h) at low-temperature of 220°C and 3.0 MPa. Detailed structure characterization and performance evaluation demonstrate the formation of ZrZnO_x mixed oxide nanoparticles on ZrZnO_x/Cu inverse catalyst as the active sites responsible for the enhanced methanol formation rate. The synergy of Zr-O-Zn species in the supported mixed oxide increase the density of interfacial sites accommodating weak and medium adsorbed CO_2 which is demonstrated to determine the methanol productivity. Transient DRIFTS studies demonstrate the oxide-metal inverse interface accelerates the reduction of adsorbed CO_2 , and oxygenate intermediates (formate and methoxy), and inhibits the formation of linear adsorbed CO^* , which accounts for the high activity and selectivity of inverse

ZrZnO_x/Cu catalyst. The structural and functional advantages of the inverse interface provide opportunities for the development of catalysts for the synthesis of high-performance, low-temperature methanol from CO_2 .

CRediT authorship contribution statement

Tang Xin: Data curation, Validation. **Qin Xuetao:** Data curation, Formal analysis. **Xu Yao:** Data curation, Formal analysis. **Gao Zirui:** Data curation, Formal analysis. **Xu Yangzhi:** Data curation, Formal analysis, Investigation, Writing – original draft. **Lin Lili:** Conceptualization, Formal analysis, Funding acquisition, Project administration, Resources, Supervision, Validation, Writing – original draft, Writing – review & editing. **Ma Ding:** Resources, Supervision, Writing – review & editing. **Zhou Wu:** Formal analysis, Resources, Writing – review & editing, Supervision. **Yao Siyu:** Resources, Validation, Writing – review & editing. **Song Chuqiao:** Validation, Writing – review & editing. **Zhang Jinrong:** Data curation, Validation. **Xie Zhiwei:** Data curation, Validation.

Declaration of Competing Interest

The authors declare the following financial interests/personal relationships which may be considered as potential competing interests: Lili Lin reports equipment, drugs, or supplies was provided by Zhejiang University of Technology.

Data availability

No data was used for the research described in the article.

Acknowledgements

This work was financially supported by the Zhejiang Provincial Natural Science Foundation of China under Grant (LR22B030003, LR21B030001), the New Cornerstone Science Foundation (D. M.), Natural Science Foundation of China (22002140), Beijing National Laboratory for Molecular Science (BNLM202011), the Beijing Outstanding Young Scientist Program (BJJWZYJH01201914430039) and the National Key R&D Program of China (2022YFA1504800). D.M. acknowledges support from the Tencent Foundation through the XPLORE PRIZE. XAS experiments were conducted at the Beijing Synchrotron Radiation Facility (BSRF). AP-XPS experiments were conducted at the Analytical Instrumentation Center of Peking University.

Appendix A. Supporting information

Supplementary data associated with this article can be found in the online version at doi:10.1016/j.apcatb.2023.123656.

References

- [1] T. Mathew, George Andrew Olah (1927–2017), *Nature* 544 (2017), 162–162.
- [2] A. Goeppert, G.A. Olah, G.K. Surya Prakash, Toward a sustainable carbon cycle: the methanol economy, *Green Chem.* (2018) 919–962.
- [3] J. Graciani, K. Mudiyanselage, F. Xu, A.E. Baber, J. Evans, S.D. Senanayake, D. Stacchiola, P. Liu, J. Hrbek, J.F. Sanz, J.A. Rodriguez, Highly active copper-ceria and copper-ceria-titania catalysts for methanol synthesis from CO₂, *Science* 345 (2014) 546–550.
- [4] G. Zhang, B. Liu, T. Wang, J. Gong, Artificial leaves for solar fuels, *Chin. J. Chem.* 39 (2021) 1450–1458.
- [5] F. Sha, Z. Han, S. Tang, J. Wang, C. Li, Hydrogenation of carbon dioxide to methanol over non-Cu-based heterogeneous catalysts, *ChemSusChem* 13 (2020) 6160–6181.
- [6] S.-T. Bai, G. De Smet, Y. Liao, R. Sun, C. Zhou, M. Beller, B.U.W. Maes, B.F. Sels, Homogeneous and heterogeneous catalysts for hydrogenation of CO₂ to methanol under mild conditions, *Chem. Soc. Rev.* 50 (2021) 4259–4298.
- [7] J. Ott, V. Gronemann, F. Pontzen, E. Fiedler, G. Grossmann, D.B. Kerschbaum, G. Weiss, C. Witte, Methanol, Ullmann's Encyclopedia of Industrial Chemistry, 2012.
- [8] J. Hansen, M. Sato, R. Ruedy, K. Lo, D.W. Lea, M. Medina-Elizade, Global temperature change, *Proc. Natl. Acad. Sci. USA* 103 (2006) 14288–14293.
- [9] C.F. Shih, T. Zhang, J. Li, C. Bai, Powering the future with liquid sunshine, *Joule* 2 (2018) 1925–1949.
- [10] T.R. Knutson, R.E. Tuleya, Impact of CO₂-induced warming on simulated hurricane intensity and precipitation sensitivity to the choice of climate model and convective parameterization, *J. Clim.* 17 (2004) 3477–3495.
- [11] A. Álvarez, A. Bansode, A. Urakawa, A.V. Bavykina, T.A. Wezendonk, M. Makkee, J. Gascon, F. Kapteijn, Challenges in the greener production of formates/formic acid, methanol, and DME by heterogeneously catalyzed CO₂ hydrogenation processes, *Chem. Rev.* 117 (2017) 9804–9838.
- [12] X. Jiang, X. Nie, X. Guo, C. Song, J.G. Chen, Recent advances in carbon dioxide hydrogenation to methanol via heterogeneous catalysis, *Chem. Rev.* 120 (2020) 7984–8034.
- [13] J. Zhong, X. Yang, Z. Wu, B. Liang, Y. Huang, T. Zhang, State of the art and perspectives in heterogeneous catalysis of CO₂ hydrogenation to methanol, *Chem. Soc. Rev.* 49 (2020) 1385–1413.
- [14] X. Liu, J. Li, N. Li, B. Li, X.-H. Bu, Recent advances on metal-organic frameworks in the conversion of carbon dioxide, *Chin. J. Chem.* 39 (2021) 440–462.
- [15] S. Kattel, B. Yan, Y. Yang, J.G. Chen, P. Liu, Optimizing binding energies of key intermediates for CO₂ hydrogenation to methanol over oxide-supported copper, *J. Am. Chem. Soc.* 138 (2016) 12440–12450.
- [16] S. Kattel, P. Liu, J.G. Chen, Tuning selectivity of CO₂ hydrogenation reactions at the metal/oxide interface, *J. Am. Chem. Soc.* 139 (2017) 9739–9754.
- [17] P. Gao, S. Li, X. Bu, S. Dang, Z. Liu, H. Wang, L. Zhong, M. Qiu, C. Yang, J. Cai, W. Wei, Y. Sun, Direct conversion of CO₂ into liquid fuels with high selectivity over a bifunctional catalyst, *Nat. Chem.* 9 (2017) 1019–1024.
- [18] S. Kuld, M. Thorhauge, H. Falsig, C.F. Elkjær, S. Helveg, I. Chorkendorff, J. Sehested, Quantifying the promotion of Cu catalysts by ZnO for methanol synthesis, *Science* 352 (2016) 969–974.
- [19] M. Behrens, F. Studt, I. Kasatkina, S. Kühl, M. Hävecker, F. Abild-Pedersen, S. Zander, F. Girgsdies, P. Kurr, B.-L. Kniep, M. Tovar, R.W. Fischer, J.K. Nørskov, R. Schlögl, The active site of methanol synthesis over Cu/ZnO/Al₂O₃ industrial catalysts, *Science* 336 (2012) 893–897.
- [20] Y. Ma, J. Wang, K.R. Goodman, A.R. Head, X. Tong, D.J. Stacchiola, M.G. White, Reactivity of a zirconia–copper inverse catalyst for CO₂ hydrogenation, *J. Phys. Chem. C* 124 (2020) 22158–22172.
- [21] M.S. Duyar, C. Tsai, J.L. Snider, J.A. Singh, A. Gallo, J.S. Yoo, A.J. Medford, F. Abild-Pedersen, F. Studt, J. Kibsgaard, S.F. Bent, J.K. Nørskov, T.F. Jaramillo, M.P.C.A. Slac National Accelerator Lab, A highly active molybdenum phosphide catalyst for methanol synthesis from CO and CO₂, *Angew. Chem. Int. Ed.* 57 (2018) 15045–15050.
- [22] J. Hu, L. Yu, J. Deng, Y. Wang, K. Cheng, C. Ma, Q. Zhang, W. Wen, S. Yu, Y. Pan, J. Yang, H. Ma, F. Qi, Y. Wang, Y. Zheng, M. Chen, R. Huang, S. Zhang, Z. Zhao, J. Mao, X. Meng, Q. Ji, G. Hou, X. Han, X. Bao, Y. Wang, D. Deng, Sulfur vacancy-rich MoS₂ as a catalyst for the hydrogenation of CO₂ to methanol, *Nat. Catal.* 4 (2021) 242–250.
- [23] K. Larmier, W.-C. Liao, S. Tada, E. Lam, R. Verel, A. Bansode, A. Urakawa, A. Comas-Vives, C. Copéret, CO₂-to-methanol hydrogenation on zirconia-supported copper nanoparticles: Reaction intermediates and the role of the metal-support interface, *Angew. Chem. Int. Ed.* 56 (2017) 2318–2323.
- [24] X. Liu, J. Luo, H. Wang, L. Huang, S. Wang, S. Li, Z. Sun, F. Sun, Z. Jiang, S. Wei, W.-X. Li, J. Lu, In situ spectroscopic characterization and theoretical calculations identify partially reduced ZnO_{1-x}/Cu interfaces for methanol synthesis from CO₂, *Angew. Chem. Int. Ed.* 61 (2022), e202202330.
- [25] C. Tang, S. Tang, F. Sha, Z. Han, Z. Feng, J. Wang, C. Li, Insights into the selectivity determinant and rate-determining step of CO₂ hydrogenation to methanol, *J. Phys. Chem. C* 126 (2022) 10399–10407.
- [26] Y. Li, Y. Zhang, K. Qian, W. Huang, Metal–support interactions in metal/oxide catalysts and oxide–metal interactions in oxide/metal inverse catalysts, *ACS Catal.* 12 (2022) 1268–1287.
- [27] J.A. Rodriguez, P. Liu, D.J. Stacchiola, S.D. Senanayake, M.G. White, J.G. Chen, Hydrogenation of CO₂ to methanol: importance of metal–oxide and metal–carbide interfaces in the activation of CO₂, *ACS Catal.* 5 (2015) 6696–6706.
- [28] O. Martin, A.J. Martín, C. Mondelli, S. Mitchell, T.F. Segawa, R. Hauer, C. Drouilly, D. Curulla-Ferré, J. Pérez-Ramírez, Indium oxide as a superior catalyst for methanol synthesis by CO₂ hydrogenation, *Angew. Chem. Int. Ed.* 55 (2016) 6261–6265.
- [29] D. Xu, X. Hong, G. Liu, Highly dispersed metal doping to ZnZr oxide catalyst for CO₂ hydrogenation to methanol: insight into hydrogen spillover, *J. Catal.* 393 (2021) 207–214.
- [30] W.-H. Feng, M.-M. Yu, L.-J. Wang, Y.-T. Miao, M. Shakouri, J. Ran, Y. Hu, Z. Li, R. Huang, Y.-L. Lu, D. Gao, J.-F. Wu, Insights into bimetallic oxide synergy during carbon dioxide hydrogenation to methanol and dimethyl ether over GaZrO_x oxide catalysts, *ACS Catal.* 11 (2021) 4704–4711.
- [31] J. Wang, C. Tang, G. Li, Z. Han, Z. Li, H. Liu, F. Cheng, C. Li, High-performance MaZrO_x (Ma = Cd, Ga) solid-solution catalysts for CO₂ hydrogenation to methanol, *ACS Catal.* 9 (2019) 10253–10259.
- [32] Y. Wang, W. Gao, K. Li, Y. Zheng, Z. Xie, W. Na, J.G. Chen, H. Wang, Strong evidence of the role of H₂O in affecting methanol selectivity from CO₂ hydrogenation over Cu-ZnO-ZrO₂, *Chem* 6 (2020) 419–430.
- [33] C. Wu, L. Lin, J. Liu, J. Zhang, F. Zhang, T. Zhou, N. Rui, S. Yao, Y. Deng, F. Yang, Inverse ZrO₂/Cu as a highly efficient methanol synthesis catalyst from CO₂ hydrogenation, *Nat. Commun.* 11 (2020) 1–10.
- [34] G. Bonura, M. Cordaro, C. Cannilla, F. Arena, F. Frusteri, The changing nature of the active site of Cu-Zn-Zr catalysts for the CO₂ hydrogenation reaction to methanol, *Appl. Catal. B Environ.* 152–153 (2014) 152–161.
- [35] G. Bonura, F. Arena, G. Mezzatesta, C. Cannilla, L. Spadaro, F. Frusteri, Role of the ceria promoter and carrier on the functionality of Cu-based catalysts in the CO₂-to-methanol hydrogenation reaction, *Catal. Today* 171 (2011) 251–256.
- [36] X. Liu, Y. Song, W. Geng, H. Li, L. Xiao, W. Wu, Cu-Mo₂C/MCM-41: an efficient catalyst for the selective synthesis of methanol from CO₂, *Catalysts* 6 (2016) 75.
- [37] X. Guo, D. Mao, G. Lu, S. Wang, G. Wu, Glycine–nitrate combustion synthesis of CuO–ZnO–ZrO₂ catalysts for methanol synthesis from CO₂ hydrogenation, *J. Catal.* 271 (2010) 178–185.
- [38] S. Li, L. Guo, T. Ishihara, Hydrogenation of CO₂ to methanol over Cu/AlCeO catalyst, *Catal. Today* 339 (2020) 352–361.
- [39] Q. Tan, Z. Shi, D. Wu, CO₂ hydrogenation to methanol over a highly active Cu-Ni/CeO₂-nanotube catalyst, *Ind. Eng. Chem. Res.* 57 (2018) 10148–10158.
- [40] K. Chen, X. Duan, H. Fang, X. Liang, Y. Yuan, Selective hydrogenation of CO₂ to methanol catalyzed by Cu supported on rod-like La₂O₂CO₃, *Catal. Sci. Technol.* 8 (2018) 1062–1069.
- [41] H. Lei, Z. Hou, J. Xie, Hydrogenation of CO₂ to CH₃OH over CuO/ZnO/Al₂O₃ catalysts prepared via a solvent-free routine, *Fuel* 164 (2016) 191–198.
- [42] Y. Wang, S. Kattel, W. Gao, K. Li, P. Liu, J.G. Chen, H. Wang, Exploring the ternary interactions in Cu-ZnO-ZrO₂ catalysts for efficient CO₂ hydrogenation to methanol, *Nat. Commun.* 10 (2019) 1–10.
- [43] F. Arena, G. Mezzatesta, G. Zafarana, G. Trunfio, F. Frusteri, L. Spadaro, Effects of oxide carriers on surface functionality and process performance of the Cu–ZnO system in the synthesis of methanol via CO₂ hydrogenation, *J. Catal.* 300 (2013) 141–151.
- [44] X. Han, M. Li, X. Chang, Z. Hao, J. Chen, Y. Pan, S. Kawi, X. Ma, Hollow structured Cu@ZrO₂ derived from Zr-MOF for selective hydrogenation of CO₂ to methanol, *J. Energy Chem.* 71 (2022) 277–287.
- [45] J. Yu, S. Liu, X. Mu, G. Yang, X. Luo, E. Lester, T. Wu, Cu-ZrO₂ catalysts with highly dispersed Cu nanoclusters derived from ZrO₂@Hkust-1 composites for the enhanced CO₂ hydrogenation to methanol, *Chem. Eng. J.* 419 (2021), 129656.
- [46] S. Wang, L. Song, Z. Qu, Cu/ZnAl₂O₄ catalysts prepared by ammonia evaporation method: improving methanol selectivity in CO₂ hydrogenation via regulation of metal-support interaction, *Chem. Eng. J.* 469 (2023), 144008.
- [47] L. Song, H. Wang, S. Wang, Z. Qu, Dual-site activation of H₂ over Cu/ZnAl₂O₄ boosting CO₂ hydrogenation to methanol, *Appl. Catal. B Environ.* 322 (2023), 122137.
- [48] Z. Shi, Q. Tan, C. Tian, Y. Pan, X. Sun, J. Zhang, D. Wu, CO₂ hydrogenation to methanol over Cu-In intermetallic catalysts: effect of reduction temperature, *J. Catal.* 379 (2019) 78–89.
- [49] A.S. Malik, S.F. Zaman, A.A. Al-Zahrani, M.A. Daous, H. Driss, L.A. Petrov, Development of highly selective PdZn/CeO₂ and ca-doped PdZn/CeO₂ catalysts for methanol synthesis from CO₂ hydrogenation, *Appl. Catal. A-Gen* 560 (2018) 42–53.
- [50] C. Zhang, H. Yang, P. Gao, H. Zhu, L. Zhong, H. Wang, W. Wei, Y. Sun, Preparation and CO₂ hydrogenation catalytic properties of alumina microsphere supported Cu-based catalyst by deposition-precipitation method, *J. CO₂ Util.* 17 (2017) 263–272.
- [51] Y. Jiang, H. Yang, P. Gao, X. Li, J. Zhang, H. Liu, H. Wang, W. Wei, Y. Sun, Slurry methanol synthesis from CO₂ hydrogenation over micro-spherical SiO₂ support Cu/ZnO catalysts, *J. CO₂ Util.* 26 (2018) 642–651.
- [52] J.M. Zuo, I. Vartanyants, M. Gao, R. Zhang, L.A. Nagahara, Atomic resolution imaging of a carbon nanotube from diffraction intensities, *Science* 300 (2003) 1419–1421.
- [53] L. Lin, S. Yao, N. Rui, L. Han, F. Zhang, C.A. Gerlak, Z. Liu, J. Cen, L. Song, S. D. Senanayake, H.L. Xin, J.G. Chen, J.A. Rodriguez, Conversion of CO₂ on a highly active and stable Cu/FeO_x/CeO₂ catalyst: Tuning catalytic performance by oxide-oxide interactions, *Catal. Sci. Technol.* 9 (2019) 3735–3742.

[54] L. Lin, S. Yao, Z. Liu, F. Zhang, N. Li, D. Vovchok, A. Martínez-Arias, R. Castañeda, J. Lin, S.D. Senanayake, D. Su, D. Ma, J.A. Rodriguez, In situ characterization of Cu/CeO₂ nanocatalysts for CO₂ hydrogenation: morphological effects of nanostructured ceria on the catalytic activity, *J. Phys. Chem. C* 122 (2018) 12934–12943.

[55] C. Morant, J.M. Sanz, L. Galán, L. Soriano, F. Rueda, An XPS study of the interaction of oxygen with zirconium, *Surf. Sci.* 218 (1989) 331–345.

[56] X. Liu, M. Wang, C. Zhou, W. Zhou, K. Cheng, J. Kang, Q. Zhang, W. Deng, Y. Wang, Selective transformation of carbon dioxide into lower olefins with a bifunctional catalyst composed of ZnGa₂O₄ and sapo-34, *Chem. Commun.* 54 (2018) 140–143.

[57] X. Wang, C. Zeng, N. Gong, T. Zhang, Y. Wu, J. Zhang, F. Song, G. Yang, Y. Tan, Effective suppression of CO selectivity for CO₂ hydrogenation to high-quality gasoline, *ACS Catal.* 11 (2021) 1528–1547.

[58] C. Zhou, J. Shi, W. Zhou, K. Cheng, Q. Zhang, J. Kang, Y. Wang, Highly active ZnO-ZrO₂ aerogels integrated with H-ZSM-5 for aromatics synthesis from carbon dioxide, *ACS Catal.* 10 (2020) 302–310.

[59] Y. Xie, J. Chen, X. Wu, J. Wen, R. Zhao, Z. Li, G. Tian, Q. Zhang, P. Ning, J. Hao, Frustrated Lewis pairs boosting low-temperature CO₂ methanation performance over Ni/CeO₂ nanocatalysts, *ACS Catal.* 12 (2022) 10587–10602.

[60] Y. Pu, Y. Luo, X. Wei, J. Sun, L. Li, W. Zou, L. Dong, Synergistic effects of Cu₂O-decorated CeO₂ on photocatalytic CO₂ reduction: surface Lewis acid/base and oxygen defect, *Appl. Catal. B Environ.* 254 (2019) 580–586.

[61] I.A. Fisher, A.T. Bell, In-situinfrared study of methanol synthesis from H₂/CO₂ over Cu/SiO₂ and Cu/ZrO₂/SiO₂, *J. Catal.* 172 (1997) 222–237.

[62] J. Wang, G. Li, Z. Li, C. Tang, Z. Feng, H. An, H. Liu, T. Liu, C. Li, A highly selective and stable ZnO-ZrO₂ solid solution catalyst for CO₂ hydrogenation to methanol, *Sci. Adv.* 3 (2017), e1701290.